26. E. C. Sittler and D. F. Strobel, *J. Geophys. Res.* **92**, 5741 (1987).
27. For electron impact excitation of Io's atmosphere in eclipse, column abundances were estimated by equating the measured brightnesses to the product of a gas-column density, an average electron density in the gas column, and an average emission rate (for the particular brightness) that depends on the effective electron temperature in the gas column. This linear relation is approximately valid if the gas column is optically thin (not true for Na optical emissions), so that created photons may escape freely without further absorption by the gas column, and if no collisional quenching occurs (not true for O optical emissions at lower altitudes). The determination of the electron temperature and density in the column is a complex problem not addressed here. Instead, we adopt a range of possible values for the electron temperature (to bound the emission rate) of 40,000 K (3.4 eV) to 60,000 K (5.2 eV) and adopt nominal plasma wake values for the electron densities of 20,000 cm^{-3} for Na and O; we also correct for the brightness for the optically thick Na column. On the basis of these temperatures, the emission rates assumed for Na were 5.4×10^{-7} to 6.8×10^{-7} photons cm^3 s^{-1} [R. Clark, N. Magee Jr., J. Mann, A. Merts, *Astrophys. J.* **254**, 412 (1982)], and the rates for O were 2.4×10^{-9} to 3.2×10^{-9} photons cm^3 s^{-1} (D. Shemansky, private communication). For SO_2 located deeper in the atmosphere, an electron temperature of 40,000 K was adopted along with an electron density of 2000 cm^{-3}. An approximate electron impact excitation rate of 1.7×10^{-10} photons cm^3 s^{-1} for the molecular band structures of SO_2 appropriate to the SSI violet filter was estimated from laboratory measurements (*6*, *25*), with guidance given by K. Becker (private communication).
28. Background plasma torus electron density as measured near Io's orbit in the plasma torus by the Voyager spacecraft is ~2000 cm^{-3} [F. Bagenal, *J. Geophys. Res.* **99**, 11043 (1994)].
29. Electron densities in the Io plasma wake as measured by the Galileo spacecraft are as high as 40,000 cm^{-3}, an order of magnitude larger than the value of ~4000 cm^{-3} measured in the plasma torus near Io [D. A. Gurnett, W. S. Kurth, A. Roux, S. J. Bolton, C. F. Kennel, *Science* **274**, 391 (1996); L. A. Frank *et al.*, *ibid.*, p. 394].
30. M. Volwerk, M. Brown, A. Dessler, B. Sandel, *Geophys. Res. Lett.* **24**, 1147 (1997).
31. M. C. Wong and W. H. Smyth, *Bull. Am. Astron. Soc.* **30**, 1117 (1998); in preparation.
32. We are grateful for informative discussions with many patient colleagues before and during the Madison, Wisconsin, meeting of the Division for Planetary Sciences of the American Astronomical Society. Particular thanks are due to C. Alexander, F. Bagenal, F. Crary, A. Dessler, F. Herbert, W. Hubbard, D. Hunten, K. Klaasen, L. Lane, M. McGrath, K. Rages, and N. Schneider.

12 March 1999; accepted 24 June 1999

Quantitative Assessment of Reactive Surface Area of Phlogopite During Acid Dissolution

Eric Rufe and Michael F. Hochella Jr.

The reactive surface area of a dissolving sheet silicate, phlogopite, was quantitatively assessed in experiments performed in the fluid cell of an atomic force microscope at room temperature and pH values of 2 and 5.7. Additional assessment was provided by surface chemical analysis and electron diffraction. Dissolution rates of phlogopite {*hk*0} edges are in the range of 10^{-10} moles per square meters per second, two orders of magnitude faster than bulk rates for this mineral. The basal {001} surfaces also show distinct reactivity, although it is short-lived before they become relatively inert. These basal surfaces are shown to leach, hydrate, and expand to an amorphous silica-enriched film.

Chemical weathering of silicate minerals exerts substantial influences on processes such as neutralization of anthropogenic acidic inputs, supplying and cycling of nutrients in natural systems, and long-term climate change by acting as a sink for atmospheric CO_2. Laboratory and field-based studies that determine dissolution rates rely on measurements of exposed mineral surface area, but unfortunately, surface area remains one of the most difficult parameters to characterize. Most often, laboratory rates are normalized to the initial surface area measured by a Brunaer-Emmett-Teller (BET) adsorption isotherm. For many silicates, no linear relation exists between rate and BET surface area (*1*), implying that not all of the measured surface area participates in the reaction at the same rate or by the same mechanism. The term "reactive surface area" is often used to distinguish the portions of the surface that dominantly contribute to measured fluxes from portions that do not. In the literature, the way in which reactive surface area is defined is variable (*2*).

To gain insight into the intricacies of mineral dissolution, others have used in situ atomic force microscopy (AFM) to examine reactions in real time on particular crystallographic faces or microtopographic features of several nonsilicate minerals (*3*). However, there are no published in situ AFM studies in which silicate dissolution rates were measured at room temperature (*4*). Our study combines in situ AFM observations of the dissolution of the mica phlogopite $[K_2Mg_6(Al_2Si_6O_{20})(OH,F)_4]$ at room temperature with x-ray photoelectron spectroscopy (XPS) and low-energy electron diffraction (LEED) analyses to quantitatively assess reactive surface area (*5*). Among silicates, micas are best suited for investigating the role of reactive surface area because mica dissolution has been well characterized by several solution studies (*6*–*9*) and because their sheetlike structure allows for the easy identification of surfaces with greatly different reactivity (*10*).

Freshly cleaved phlogopite {001} surfaces were etched in HF to produce crystallographically controlled etch pits (*11*) and then placed in an AFM fluid cell to which an aqueous solution was introduced (*12*). Dissolution proceeds by the removal of material from the etch pit walls (*13*) (Fig. 1). Etch pits retain the same morphology while dissolving, indicating that each etch pit wall retreats at essentially the same rate. Additionally, no new etch pits nucleate on {001} surfaces. We have imaged the same region of the surface at various times over the course of several days, and the volume of phlogopite removed from a particular etch pit is measured at each time interval (*14*). XPS analysis shows decreasing K/Si, Al/Si, Mg/Si, and F/Si atomic ratios within the first 24 hours of reaction. Because Mg, Al, and K are preferentially removed with respect to Si, the dissolution rates determined from these AFM observations are compared to dissolution rates calculated from Si release reported in solution studies. Dissolution rates were calculated as

$$\text{rate} = \frac{(\Delta V/V_m)}{\text{SA}(t)} \quad (\text{mol m}^{-2}\ \text{s}^{-1}) \qquad (1)$$

where ΔV is the volume of phlogopite removed from the etch pit, V_m is the molar volume of the phlogopite (based on a complete formula unit), t is the time interval, and SA is surface area. Dissolution rates of pit edges measured in this study were normalized to the initial SA of the {*hk*0} edges (*15*) (Fig. 2). However, dissolution rates of micas in the literature are normalized to the initial BET-measured SA of particles, which includes both {00l} and {*hk*0} surfaces. To compare the rates calculated from an etch pit directly to the rates reported in the literature, it is necessary to construct an imaginary particle with the same edge surface area as that of the etch pit. This was achieved by treating each etch pit as a "negative" particle with the same lateral dimensions as follows. An etch pit Z nanometers deep of size $A_{initial}$ expands to size A_{final} during time t. Assume that this is equivalent to a particle Z nanometers thick of size A_{final} shrinking to size $A_{initial}$ during time t. The equivalent particle is constructed so that

Department of Geological Sciences, Virginia Polytechnic Institute and State University, Blacksburg, VA 24061–0420, USA.

$$A_{\text{total,initial}} = 2A_{\text{EP,final}} + (ZP_{\text{final}})\ (\text{nm}^2) \quad (2)$$

$$A_{\text{total,final}} = 2A_{\text{EP,initial}} + (ZP_{\text{initial}})\ (\text{nm}^2) \quad (3)$$

where A_{EP} is the cross-sectional area of the etch pit and P is the etch pit perimeter. The total surface area determined in this way provides a geometric estimate of a BET equivalent surface area (*16*). Dissolution rates calculated from AFM images were then normalized to the total surface area of the equivalent particle for each etch pit. The dissolution rates determined in this way are in the range of reported trioctahedral mica dissolution rates, whereas dissolution rates normalized to edge surface area are ~100 times as fast (*15*) (Fig. 2).

Long-term in situ AFM imaging of phlogopite in contact with a HCl solution (pH 2) provides evidence of the reactivity of phlogopite {001} surfaces. Measured layer thicknesses of all layers exposed in a stepped etch pit (such as that shown in Fig. 1) are initially ~1.0 nm, corresponding to the thickness of one fundamental layer in the phlogopite structure. The layer thickness of the deeper layers remained constant during the 127 hours when they were in contact with the HCl (pH 2) (*15*). However, between 39 and 63 hours, the thickness of the top layer increased from ~1.0 to ~1.8 nm (Fig. 3). After 127 hours, tip-induced erosion was observed on the top layer only (*15*). Material was removed with continued scanning, leaving a persistent, uneven film with an average thickness of ~1.2 nm. This increase in layer thickness was observed at two other locations on the sample surface and is a pervasive feature. It is unlikely that the solution in the fluid cell reached saturation with respect to a secondary phase, ruling out the possibility of precipitation accounting for the increase in layer thickness (*17*). XPS performed after the sample was in contact with HCl (pH 2) for 127 hours reveals that atomic concentrations of K, Al, Mg, and F are severely depleted and the top layer is composed of essentially only Si and O (*18*). Not surprisingly, LEED analysis performed on this sample yielded no diffraction spots, indicating that the surface region of the sample is now amorphous.

The observed layer volume change may be explained by depolymerization and repolymerization reactions occurring during leached layer formation. The general leached layer model consists of three steps (*19*). The first, sometimes referred to cation exchange, involves the rapid exchange of alkali and alkaline-earth cations for hydrogen or hydronium. The second involves depolymerization reactions, in which bridging Si-O-Si and Si-O-Al linkages are hydrolyzed, allowing the layer to expand. The third step is spontaneous repolymerization reactions in which neighboring Si-OH groups cross-link to reform Si-O-Si linkages, ejecting hydrogen and water. This may cause the layer to contract.

Mica dissolution is thought to be dominated by an edge attack mechanism (*6–9*). In acidic solution, interlayer and octahedral cations are selectively leached through {*hk*0} surfaces forming an altered silica-enriched rim. Dissolution reaches steady state when the removal of silica from the altered edges is matched by diffusion of interlayer and octahedral cations parallel to the sheets, through the altered rim. However, acid hydrolysis studies of expandable clays provide evidence for the leaching of octahedral cations perpendicular to the sheets, through the ditrigonal cavities of the {001} surface by a mechanism referred to as gallery access (*20*). Our observations that the {001}

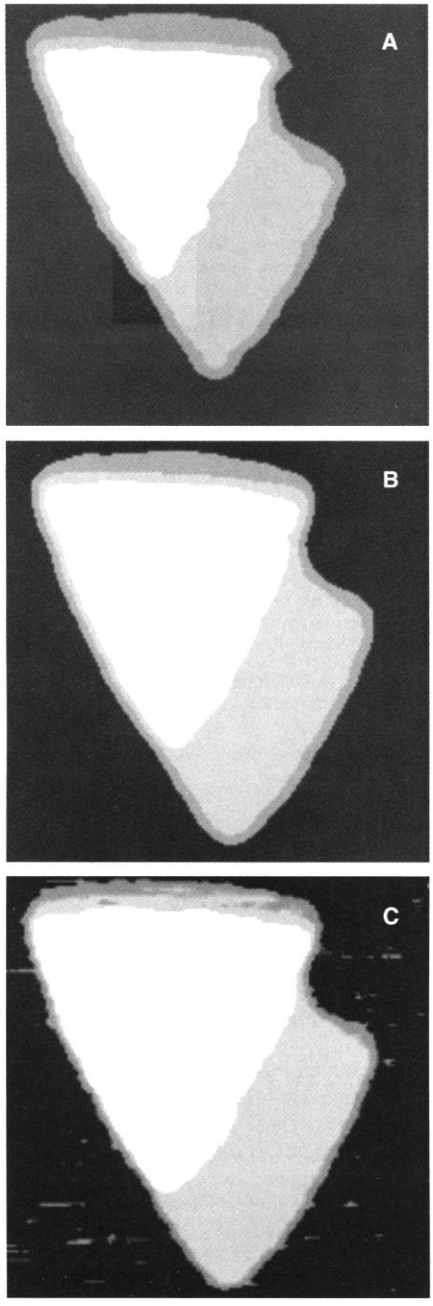

Fig. 1. AFM image of phlogopite {001} surfaces. (**A**) After the surfaces were etched in HF, showing typical initial morphology of etch pits. The darkest layer is the highest topographic layer (the original {001} surface before etching). Each successive lighter layer is 1.0 nm lower. The pits are triangular and flat bottomed. The same etch pit after the phlogopite was in contact with HCl (pH 2) for (**B**) 39 and (**C**) 63 hours. All three images are the same scale; each image is 625 nm wide.

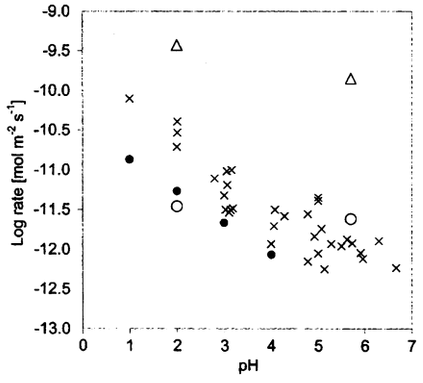

Fig. 2. Comparison of phlogopite dissolution rates (open circles and triangles) determined in our study to reported phlogopite (solid circles) (*7*) and biotite (crosses) (*6–8*) dissolution rates. Dissolution rates of biotite (a closely related trioctahedral mica) are included because there are few published phlogopite rates. Open triangles indicate rates normalized to the {*hk*0} edge surface area. Open circles indicate rates normalized to total surface area. Average {*hk*0} SA normalized rates are $3.7 \pm 1.3 \times 10^{-10}$ mol m^{-2} s^{-1} at pH 2 and $1.4 \pm 0.5 \times 10^{-10}$ mol m^{-2} s^{-1} at pH 5.7. Average total SA normalized rates are $3.5 \pm 2.3 \times 10^{-12}$ mol m^{-2} s^{-1} at pH 2 and $2.4 \pm 1.2 \times 10^{-12}$ mol m^{-2} s^{-1} at pH 5.7.

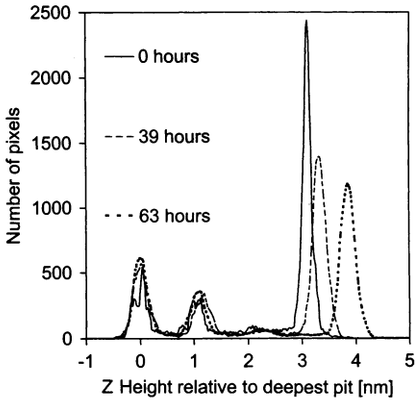

Fig. 3. Distribution of topography in images shown in Fig. 1. *Z* height 0.0 is the topographic level corresponding to the floor of the etch pit seen in Fig. 1. Peak separation measures step height (or layer thickness). The peaks at 0.0 and 1.0 nm remain constant, indicating that these deeper layers retain the same thickness. The peak representing the top layer shifts from 3.0 to 3.8 nm, indicating that this layer has expanded from 1.0 to 1.8 nm in thickness.

surface undergoes a compositional change and expansion indicate that exposed {00l} surfaces also participate in the dissolution process, at least initially.

This study has provided directly measured dissolution rates for surfaces on phlogopite, a silicate mineral, at room temperature. It has also shown that all phlogopite surfaces are reactive, including its basal surfaces. Each surface of phlogopite, or any other mineral, must behave according to the particular atomic structure, composition, and microtopography of that surface. Furthermore, the dissolution of each surface has a temporal dependence, although this effect may only be substantially variable in the early stages of dissolution. Finally, external factors must also come into play (for example, local conditions and proximal flow regimes), especially in natural settings (*21*). The concept and use of reactive surface area in silicate dissolution studies is now changing. It seems that, at least in the most favorable cases, the reactivity of various surface components can be cataloged and quantified. This opens the door to a new generation of rate equations and, ultimately, to a much better understanding of how minerals dissolve and influence our environment.

References and Notes

1. S. L. Brantley and Y. Chen, in *Chemical Weathering Rates of Silicate Minerals*, vol. 31 of *Reviews in Mineralogy*, A. F. White and S. L. Brantley, Eds. (Mineralogical Society of America, Washington, DC, 1995), chap. 4; A. F. White and M. L. Peterson, in *Chemical Modeling of Aqueous Systems II*, vol. 416 of *ACS Symposium Series*, D. C. Melchior and R. L. Bassett, Eds. (American Chemical Society, Washington, DC, 1990), chap. 35.
2. Some authors define reactive surface area as the area occupied by high-energy sites, such as defects and dislocation outcrops [W. H. Casey, M. J. Carr, R. A. Graham, *Geochim. Cosmochim. Acta* **52**, 1545 (1988)]. In surface complexation modeling, reactive sites consist of particular atomic arrangements where ligand adsorption and activated complex formation occur [C. M. Koretsky, D. A. Sverjensky, N. Sahai, *Am. J. Sci.* **298**, 349 (1998)]. Microscopic studies of the mineral-solution interface indicate that coordinatively unsaturated microtopographic configurations, such as kinks and steps, consist of the most reactive portion of a mineral surface [M. F. Hochella Jr., in *Mineral Surfaces*, vol. 5 of *Mineralogical Society Series*, D. J. Vaughan and R. A. D. Pattrick, Eds. (Chapman & Hall, New York, 1995), chap. 2]. In field-based studies, reactive surface area is the portion of the total mineral surface area that is in hydrologic contact with the system under study [J. I. Drever and D. W. Clow, in *Chemical Weathering Rates of Silicate Minerals*, vol. 31 of *Reviews in Mineralogy*, A. F. White and S. L. Brantley, Eds. (Mineralogical Society of America, Washington, DC, 1995), chap. 10].
3. G. Jordan and W. Ramansee, *Geochim. Cosmochim. Acta* **60**, 5055 (1996); Y. Liang, D. R. Baer, J. M. McCoy, J. E. Amonette, J. P. LaFemina, *ibid.*, p. 4883; A. Putnis, J. L. Junta-Rosso, M. F. Hochella Jr., *ibid.* **59**, 4623 (1995).
4. Real-time in situ dissolution of clay particles has been observed with AFM (D. Bosbach *et al.*, in preparation).
5. AFM images were collected with a NanoScope IIIa controller (Digital Instruments, Santa Barbara, CA) operating with TappingMode imaging and oxide-sharpened Si_3N_4 tips. Several images were collected in succession and compared to check for scanner drift and tip-induced erosion. XPS measurements were performed with a PHI 5400 x-ray photoelectron spectroscopy system (Perkin-Elmer, Eden Prairie, MN) using Al Kα radiation (1486.6 eV). Measurements were collected at 0°, 55°, and 75°, corresponding to approximate depths of analysis of 8.0, 4.5, and 2.0 nm, respectively [M. F. Hochella Jr. and A. H. Carim, *Surf. Sci.* **197**, L260 (1988)]. LEED spot patterns were collected with four-grid reverse-view LEED optics (OMICRON, Taunusstein, Germany) at beam energies between 50 and 150 eV.
6. M. Malmstrom and S. Banwort, *Geochim. Cosmochim. Acta* **61**, 2779 (1997).
7. B. E. Kalinowski and P. Schweda, *ibid.* **60**, 367 (1996).
8. J. G. Acker and O. P. Bricker, *ibid.* **56**, 3073 (1992).
9. See a review by K. L. Nagy, in *Chemical Weathering Rates of Silicate Minerals*, vol. 31 of *Reviews in Mineralogy*, A. F. White and S. L. Brantley, Eds. (Mineralogical Society of America, Washington, DC, 1995), chap. 5, and references therein.
10. In a comparative study of the reactivity of different surfaces on biotite, the edges were found to dissolve ~250 times as fast as the basal surfaces [M.-P. Turpault and L. Trotignon, *Geochim. Cosmochim. Acta* **58**, 2761 (1994)].
11. Etching was achieved by immersing the sample in 49% HF for 3 s, followed by a thorough rinsing with distilled-deionized H_2O. XPS analysis shows no increase in F content of the near surface, and all atomic ratios remain the same as those of unetched phlogopite, indicating that HF is not entering the structure. The LEED pattern is consistent with freshly cleaved phlogopite.
12. The solution [HCl (pH 2) or distilled water (pH 5.7) equilibrated with atmospheric CO_2] was introduced by means of a syringe and pumped at 10 ml $hour^{-1}$ with a low-flow peristaltic pump. Pumping was suspended during AFM image acquisition. When not imaging, the tip was withdrawn. Image quality degrades within 24 to 48 hours at pH 5.7, precluding long-term in situ experiments at this pH.
13. M. F. Hochella Jr., J. F. Rakovan, K. M. Rosso, B. R. Bickmore, E. Rufe, in *Mineral-Water Interfacial Reactions: Kinetics and Mechanisms*, vol. 715 of *ACS Symposium Series*, D. C. Sparks and T. J. Grundl, Eds. (American Chemical Society, Washington, DC, 1998), pp. 37–56.
14. This is achieved by using standard image analysis routines to measure the area, perimeter, and volume for each etch pit imaged. [J. C. Russ, *The Image Processing Handbook* (CRC Press, Ann Arbor, MI, ed. 3, 1995)].
15. Etch pit dimensions and dissolution rates are available at www.sciencemag.org/feature/data/1040546.shl.
16. A. Nonaka [*J. Colloid Interface Sci.* **99**, 335 (1984)] reports a roughness value (that is, ratio of BET surface area to geometric surface area) for mica of 1.08, so this estimate of BET-equivalent area should be reasonable.
17. A high flow rate coupled with a slow dissolution rate prevents saturation with respect to secondary phases at pH 2. Reaching saturation with respect to amorphous silica, for example, would require >100 layers of phlogopite to dissolve in static fluid filling the 0.03-ml fluid cell.
18. At 55°, Mg/Si decreases from 1.0 to 0.25, and Al/Si decreases from 0.33 to 0.21. K 2p and F 1s peaks are not discernable above the background. Si/O increases from 0.22 to 0.49.
19. W. H. Casey and B. Bunker, in *Mineral-Water Interface Geochemistry*, vol. 23 of *Reviews in Mineralogy*, M. F. Hochella Jr. and A. F. White, Eds. (Mineralogical Society of America, Washington, DC, 1990), chap. 10.
20. H. Kaviratna and T. J. Pinnavaia, *Clays Clay Miner.* **42**, 717 (1994).
21. M. F. Hochella Jr. and J. F. Banfield, in *Chemical Weathering Rates of Silicate Minerals*, vol. 31 of *Reviews in Mineralogy*, A. F. White and S. L. Brantley, Eds. (Mineralogical Society of America, Washington, DC, 1995), chap. 8.

22. We thank U. Becker, B. R. Bickmore, D. Bosbach, J. D. Rimstidt, J. L. Rosso, and K. M. Rosso for helpful discussions. We also thank B. R. Bickmore for developing some of the image analysis routines used in this study. The phlogopite sample was obtained from the Museum of Geological Sciences at Virginia Tech (sample HB-1246). Funding for this research was generously provided by the Petroleum Research Fund, administered by the American Chemical Society (grants PRF 31598-AC2 and 34326-AC2) and NSF (grants EAR-9527092 and EAR-9628023). This manuscript benefited from two anonymous reviewers.

1 April 1999; accepted 11 June 1999

Late Miocene Atmospheric CO_2 Concentrations and the Expansion of C_4 Grasses

Mark Pagani,*† Katherine H. Freeman, Michael A. Arthur

The global expansion of C_4 grasslands in the late Miocene has been attributed to a large-scale decrease in atmospheric carbon dioxide (CO_2) concentrations. This triggering mechanism is controversial, in part because of a lack of direct evidence for change in the partial pressure of CO_2 (pCO_2) and because other factors are also important determinants in controlling plant-type distributions. Alkenone-based pCO_2 estimates for the late Miocene indicate that pCO_2 increased from 14 to 9 million years ago and stabilized at preindustrial values by 9 million years ago. The estimates presented here provide no evidence for major changes in pCO_2 during the late Miocene. Thus, C_4 plant expansion was likely driven by additional factors, possibly a tectonically related episode of enhanced low-latitude aridity or changes in seasonal precipitation patterns on a global scale (or both).

Instability in Miocene climates is detailed by extensive stable isotope records (*1*) and is associated with turnovers in marine (*2*, *3*) and terrestrial biota (*4*), sea-level variability (*5*), and changes in surface- (*2*) and deep-water circulation (*6*). Short- and long-term climatic patterns are thought to reflect changes in CO_2 concentrations (*7*–*9*) or tectonically driven readjustments in ocean circulation (*6*, *10*). In particular, high-latitude climates gradually warmed during the early to middle Miocene [~24 to 15 million years ago (Ma)] and then